# Preliminary Error Budget for an Optical Ranging System: Range, Range Rate, and Differenced Range Observables

W. M. Folkner and M. H. Finger
Tracking Systems and Applications Section

*Future missions to the outer solar system or human exploration of Mars may use telemetry systems based on optical rather than radio transmitters. Pulsed laser transmission can be used to deliver telemetry rates of about 100 kbits/sec with an efficiency of several bits for each detected photon. This article discusses navigational observables that can be derived from timing pulsed laser signals. Error budgets are presented based on nominal ground station and spacecraft-transceiver designs. Assuming a pulsed optical uplink signal, two-way range accuracy may approach the few-centimeter level imposed by the troposphere uncertainty. Angular information can be achieved from differenced one-way range using two ground stations with the accuracy limited by the length of the available baseline and by clock synchronization and troposphere errors. A method of synchronizing the ground station clocks using optical ranging measurements is presented. This could allow differenced range accuracy to reach the few-centimeter troposphere limit.*

## I. Introduction

Advanced spacecraft require increasingly higher telemetry rates to cope with the needs of more sophisticated scientific instruments. Increasing the frequency of the telemetry carrier generally increases the data rate by providing more power at the detector due to reduced diffraction-limited beam divergence. Changing the carrier from the radio to the optical band can improve the received-to-transmitted power ratio due to the much higher frequency. Coupled with conversion efficiency approaching 50 percent for solid-state lasers, there is a potential for reduced spacecraft weight and power requirements for a given data rate [1]. New modulation techniques can be employed with an optical telemetry system. Pulse-position modulation (PPM), in which characters are encoded in the arrival times of narrow laser pulses, is being considered for use in the outer solar system.

Spacecraft navigation is based largely on observables derived from the telemetry system. Several observables are available from an optical PPM system. In this article, the potential accuracy of tracking observables derived from the timing information available from PPM signals is examined. These observables include two-way range and differenced one-way range (DOR). The range rate can be derived from the range measurements. These observables correspond to existing radio metric data types.

While optical telemetry systems are under development, there may be a number of "hybrid" missions where normal radio metric data are available. The optical tracking techniques should be explored during these missions since they may provide greater accuracy and may eventually provide stand-alone capability. A new tracking data type is an astrometric angular measurement between the spacecraft and a target solar-system body.[1] Since most solar-system bodies are not bright in the radio band, this data type has not previously been available. Astrometric tracking is not considered in this article.

Optical systems suffer much more than radio systems from weather and daytime degradation. Sufficient reduction of daytime skylight may be attained through use of sun shades and narrow bandpass filters [2,3]. The use of a number of sites a few hundred kilometers apart may provide adequate freedom from cloud cover. Investigations into cloud statistics at candidate sites are proceeding [4]. The alternative to acceptable ground stations is the use of an orbiting communications facility. This alternative will be more expensive and more difficult to maintain and upgrade. For the purposes of this article, it is assumed that ground stations will provide adequate communications capability. The optical tracking observables will be available under standard telemetry conditions, including clear daytime conditions.

The accuracy of optical observables will depend on the parameters of the telemetry system. However, there is as yet no well defined design of a complete optical telemetry system. A nominal system providing a data rate of 100 kbits/sec from Saturn has been the basis of studies for an optical spacecraft transceiver and ground receiving stations [2,3,5]. The parameters from these previous studies have been adopted here, with extensions where necessary, to examine the tracking observable accuracies. Some specific areas where additional assumptions were made are the definition and performance of the detectors for the spacecraft and ground station and the effect of the troposphere on the uplink signals. Given signal-to-noise ratio and detector performance sufficient for telemetry operation, the DOR accuracy is likely to be limited by troposphere and clock synchronization uncertainties, while two-way range accuracy should be limited by troposphere and spacecraft transceiver uncertainties. Designing the transceiver with attention to minimization of the range error may allow two-way range accuracy of $\leq 10$ cm to be achieved.

The following section briefly describes the PPM telemetry system and the method proposed for deriving two-way range and DOR. The parameters of the telemetry system assumed for this study are presented in Section III. The errors in the optical tracking observables include the uncertainty in pulse arrival time (at the spacecraft and at the ground station), instrumental delay uncertainties, media delay uncertainty, and clock error. Station location and Earth orientation uncertainties are not included, since for spacecraft navigation these errors are counted separately. The uncertainty in the pulse arrival time is due to photon statistics and instrumental effects. The photon statistical errors are discussed in Section IV. The success of satellite laser ranging (SLR) suggests that the instrumental errors can reach the subcentimeter level. In Sections V, VI, and VII, preliminary error budgets for the optical tracking observables are presented. Synchronization of ground station clocks is an important error source for DOR. In Section VIII, a method to synchronize ground station clocks through a combination of two-way and three-way range measurements is presented.

## II. Range Measurements from the PPM Telemetry System

Figure 1 is a simplified diagram of the components of the optical telemetry system. The spacecraft laser transmits pulses at a wavelength of 532 nm through the dichroic splitter and main objective towards the Earth. The beam diameter at the Earth is comparable to the diameter of the Earth (for the nominal spacecraft system at Saturn). This requires the spacecraft to transmit to the predicted position of the Earth. The spacecraft main objective is used to collect incoming light from the Earth, most of which is reflected by the two dichroic splitters into the tracking detector. The position of the Earth's image on the tracking detector is used to determine the location of the Earth and compute the correct pointing angle for transmission. Steering optics (not shown) are used to deflect the outgoing laser beam by the correct amount. The tracking detector uses the visible portion of the incoming light. The infrared portion is transmitted by the second dichroic splitter for use by the uplink detector.

The ground receiver derives the telemetry from timing pulse arrivals. Since no imaging is necessary, the receiver can consist of a number of objectives added incoherently. The Strawman receiver design consists of segments of about 1-m diameter with a total collecting area equivalent to a 10-m-diameter collector. A narrow band filter (not shown) is inserted prior to the downlink detector to subtract most of the light from the sky.

The uplink transmitter sends narrow pulses of infrared light at 1060 nm for the uplink telemetry. The

[1] G. Null, "Unique Earth-based Optical-Navigation Data Types," JPL IOM 314.5-1292 (internal document), Jet Propulsion Laboratory, Pasadena, California, September 2, 1988.

uplink transmitter need not be larger than 10 cm in diameter since the troposphere smears the uplink beam by an amount corresponding to the diffraction limit of an objective diameter of 10 cm or smaller, depending on weather conditions. For this article, an uplink data rate of 0.5 kbits/sec with 10-ns-pulse widths and a PPM decoder on the spacecraft has been assumed. However, for ranging purposes, no telemetry is required; only the ability to detect uplink pulses and trigger the downlink laser is necessary. Even if no optical uplink telemetry capability is needed, the addition of an uplink detector for ranging purposes could be included.

PPM encoding/decoding is illustrated in Fig. 2. A clock is used to define slots (time intervals) of equal width. The transmitting laser is triggered in the middle of slot $n$, where $n$ ranges from 1 to the alphabet size $2^N$. The receiving station clock is synchronized to the transmitter clock to determine the time corresponding to the beginning of slot 1. The detection of the pulse determines which PPM symbol (out of $2^N$ possible symbols) has been received. The difference between the center of the received pulse and the center of the slot is measured and used to keep the receiver clock synchronized with the telemetry stream.

The detection of each pulse determines $N$ bits of information. In principle, $N$ bits can be received for a single detected photon. The desired telemetry rate and slot width determine the number of pulses per second required. The telemetry also includes error correction bits to achieve a given error tolerance. The nominal downlink requirements are a 100 kbits/sec data rate and a bit error rate of $10^{-3}$. Employing 7/8 Reed-Soloman encoding with these requirements results in a raw telemetry rate of 114.35 kbits/sec.[2] With 8 bits per PPM symbol, 14,294 pulses/sec are needed to send 114.35 kbits/sec.

Figure 3 is a functional block diagram of the telemetry and ranging system. It is proposed that for ranging purposes the spacecraft can be put into a mode in which a single downlink pulse is sent for each detected uplink pulse. This will interrupt the telemetry for the period of the measurement, which may be on the order of a few seconds. In this mode, the downlink pulse rate will be reduced to the uplink rate. To avoid delay errors associated with the PPM decoding and encoding steps, a bypass switch can be used in ranging operation. DOR measurements can be done by sampling the regular downlink telemetry.

A two-way range measurement is derived from the time interval between the transmission of an uplink pulse and the reception of the corresponding downlink pulse. The time of the uplink pulse is determined by deflecting part of the uplink signal into a separate detector and time tagging the output following an amplifier and shaping circuit. This method avoids the uncertainty in the laser response that might be a problem for a high-power uplink laser. The spacecraft receives the uplink pulse at the uplink detector. The shaping amplifier produces a signal that, fed through the range switch, can be used to trigger the laser. The signal adder allows the spacecraft laser to be triggered by uplink ranging pulses or downlink telemetry signals. The returned ranging pulse is detected by the downlink detector, followed by an amplifier, and time tagged. A two-way range measurement is derived from the difference between the time tags for each uplink pulse and its corresponding downlink pulse. Range ambiguities can be easily resolved by imposing a pattern (ranging code) on the times of the uplink pulses.

Many error terms will be reduced by the square root of the number of measurements, so that in a short time the range error will be dominated by systematic effects such as the error in the troposphere model and instrumental biases. The number of measurements per second will be set by the uplink laser pulse rate. In the example included here, the uplink pulse rate of 63 Hz supplies a telemetry rate of 0.5 kbits/sec given a PPM alphabet size of 256 (8 bits/pulse).

DOR would be derived by time tagging downlink pulses from the downlink telemetry stream at two ground stations. The DOR error is likely to be dominated by the uncertainty in clock synchronization between the two stations. The angular accuracy depends on the separation of the ground stations. For the diffraction-limited spacecraft objective of 30-cm diameter, the beam diameter at the Earth is 650 km when the spacecraft is 1 AU from Earth. The beam diameter increases to 6500 km at 10 AU. However, a focal length adjustment may be included on the spacecraft to optimize power delivered to the ground station. This possibly could be used to deliberately spread the beam for DOR measurements to increase the available baseline at some cost in signal-to-noise ratio.

## III. Nominal System Parameters

The parameters listed in Table 1 for the PPM downlink from Saturn are taken from the McDonnell Douglas transceiver study [5] and Kerr's ground station design [2,3]. The Communications Systems Research Section optical link analysis program [6] was employed to design a nominal uplink at 0.5 kbits/sec. The uplink parameters assumed for this telemetry system are given in Table 2. The

[2] W. K. Marshall, "Using the Link Analysis Program with R-S Encoded Links," JPL IOM 331-86.6-202 (internal document), Jet Propulsion Laboratory, Pasadena, California, August 1,1986.

uplink power received will be affected by beam steering and spreading due to the troposphere. These effects were estimated by using a small uplink transmitter objective (corresponding to 2-arcsec seeing) along with 0.5-arcsec steering bias and 1-arcsec steering jitter.

The parameters listed in Tables 1 and 2 have been chosen to provide a sufficient signal-to-noise ratio to meet telemetry rate requirements in the absence of detector limitations. The important parameters from the ranging perspective are the slot width, the number of signal photons received per pulse, and the number of background photons per slot. The downlink background rate is due to the daytime sky irradiance. Here a value of 100 W/($\mu$m $m^2$ steradian) at 532 nm was used for the sky spectral irradiance [7]. Including the radiance of Saturn as a background source would increase the background rate by less than 5 percent [8]. The uplink background rate is due to Earthshine. The spacecraft objective, which is assumed to be diffraction limited, resolves the Earth out to 9.9 AU. That is, the Earth fills the field of view of the spacecraft telescope out to that distance. Thus, the background power received by the spacecraft is independent of the distance from the Earth up to that point. Therefore, the Earth has been treated as an extended background source with spectral radiance 6.5 W/($\mu$m $m^2$ steradian) at 1060 nm [9]. The background due to scattered sunlight, which will depend on the sun shield design and objective quality for the spacecraft transceiver, has been ignored.

The proper detectors for use at the ground station and on the spacecraft have yet to be determined. Photomultiplier tubes (PMTs) are used in satellite and lunar laser ranging with timing accuracy better than the media error [10]. Daytime SLR has been performed with PMTs with good accuracy, although the gain of the PMT was reduced due to the high background rate [11]. The quantum efficiency of some PMTs at the downlink wavelength (532 nm) is about 0.1 and may be high enough for telemetry operation; if not, the quantum efficiency may be increased through internal reflection techniques [12]. At the uplink wavelength (1060 nm), the quantum efficiency of PMTs is too low for use on the spacecraft. Instead, over-biased avalanche photodiodes (APDs) are being investigated as candidate detectors. These devices can have large quantum efficiency at the uplink wavelength [13], very fast response time [14], and low dark-count rate [15]. The dead time of these APDs will probably make them unsuitable for use on the ground station, but, since the uplink background rate is lower, the APD dead time may be tolerable on the uplink.

For the rest of this article, the ground station detector is assumed to be a PMT with no dead time, linear response, and an impulse response time much less than 10 nsec. The uplink detector is assumed to be an APD with fast response time and dead time that is long compared to the PPM symbol length (2.56 $\mu$sec). The APD is activated shortly before the expected time of arrival of the PPM symbol and detects the arrival of the next incident photon.

## IV. Photon Statistics of Pulse Arrival

The error in determining the time of pulse arrival depends on the detection strategy and the instrumental parameters. This section presents the errors due to photon statistics for particular uplink and downlink pulse-detection algorithms. These algorithms are shown to be adequate to derive precise range observables; they may not suffice to derive the needed telemetry accuracy.

Statistical variations in the time of arrival of the first photon in an uplink pulse result in jitter in the time of transmission of the corresponding downlink pulse, while background photons at the spacecraft can result in premature downlink pulses. Since the background rate at the spacecraft is relatively low, the detector can trigger on the first detected photon. The transmitted pulse shape is expected to have a flat top centered in the slot with some rise and fall time. A particular example of a normalized pulse shape is shown in Fig. 4, which is given by

$$f(\tau) = \frac{1}{7 \text{ nsec}} \times \begin{cases} 0 & \tau < 0 \\ \tau/2 \text{ nsec} & 0 < \tau < 2 \text{ nsec} \\ 1 & 2 \text{ nsec} < \tau < 7 \text{ nsec} \\ (9 \text{ nsec} - \tau)/2 \text{ nsec} & 7 \text{ nsec} < \tau < 9 \text{ nsec} \\ 0 & 9 \text{ nsec} < \tau \end{cases} \quad (1)$$

which defines a 9-nsec-wide pulse to fit inside the 10-nsec slot. Detecting the first photon instead of estimating the center of the pulse introduces a bias that can be calibrated out.

To determine the photon statistical error in triggering on the first detected photon, the probability distribution of the time of detection of the first photon is derived. The detector is activated at time $t_{\text{gate}}$ before $t_0$, the time of arrival of the pulse. Let $P_1(t)$ be the probability that the first photon arrives at time $t$, where $t_{\text{gate}} < t$. The mean number of detected photons expected in the interval from $t_{\text{gate}}$ to a later time $t_1$ is

$$N(t_1) = \int_{t_{gate}}^{t_1} [B_u + S_u f(t - t_0)]dt \qquad (2)$$

where $B_u$ is the background rate as seen by the uplink detector and $S_u$ is the average number of detected signal photons per pulse. According to Poisson statistics, the probability of no photons being detected in the interval $t_{gate}$ to $t_1$ is $e^{-N(t_1)}$ [16]. Then the integral of $P_1(t)$ is given by

$$\int_{t_{gate}}^{t_1} P_1(t)dt = 1 - e^{-N(t_1)} \qquad (3)$$

since the probability that the first photon arrived by $t_1$ is 1 minus the probability of no photons arriving before time $t_1$. Thus, $P_1(t)$ is given by

$$P_1(t) = \frac{\partial}{\partial t_1}\left(1 - e^{-N(t_1)}\right)\Big|_{t_1=t} \qquad (4)$$

The distribution $P_1(t)$ for the pulse shape given above and the uplink source and background rates given in Section II are shown in Fig. 5. The value of 1.2 $\mu$sec for $t_0 - t_{gate}$ has been used as an example. Nine-tenths percent of the distribution is due to the detection of a background photon before the pulse's arrival, while less than one-tenth percent is due to background photons being detected after no signal photons were detected. The remaining portion of the distribution is contained in a narrow peak with a mean of 2.1 nsec after the pulse arrival and a variance of (1.3 nsec)$^2$. This error will decrease as 1 over the square root of the number of measurements.

An important consequence of the first-photon detection algorithm is that the mean of the distribution depends on the power level of the received signal. If the number of detected photons per pulse changes by 10 percent, the distribution mean changes by 0.19 nsec. An estimate of the detected uplink power level can be made by analyzing the shape of the range distribution. Alternatives to doing this include shortening the uplink pulses, increasing the uplink laser power (which lowers the first photon shift with respect to power level change), or using a detector that can respond to more than one photon per uplink pulse.

At the ground station, the background rate is too high to simply detect the arrival of the first photon in the pulse. If the arrival of each photon could be time tagged, the maximum likelihood estimator could be used to estimate the pulse arrival time [17]. This procedure consists of maximizing the likelihood function $L$ where

$$ln(L) = \sum_{k=1}^{n} ln\left(1 + f(t_k - \hat{t}\,)\frac{S_d}{B_d}\right) + \text{constant} \qquad (5)$$

where $L$ is the a posteriori probability that a set of photon detection times $t_k$ would result from a pulse arriving at time $\hat{t}$ given the background rate $B_d$, the expected number of photons in the pulse $S_d$, and the number $n$ of photons detected in the gating window.

Although time tagging the arrival of each photon might be prohibitively difficult, Eq. (5) can be viewed as specifying an optimal pulse-shaping filter that has an impulse response proportional to $ln(1 + f(t)S_d/B_d)$. Detection of the peak time of a signal resulting from the detector filtered in this manner results in the maximum likelihood estimate of the pulse arrival time.

The statistical error in this estimation of the pulse arrival time is given by [17]

$$\frac{1}{\sigma_{\hat{t}}^2} = \int \frac{\left[S_d \frac{\partial f(t)}{\partial t}\right]^2}{B_d + S_d f(t)} dt \qquad (6)$$

For the pulse shape given by Eq. (1) and the downlink signal and background rates given in Section II, this results in a single measurement timing error of 0.38 nsec.

## V. Two-Way Range Error Budget

An analysis of detected minus predicted downlink pulse arrival times will reflect the combined effects of error in the time tagging of the uplink pulse, pulse detection jitter at the spacecraft, the downlink pulse arrival time error, and media delay errors. A small percentage of the differences will be spread out in a flat distribution due to background photons at the spacecraft, but 99 percent will be contained in a central peak. Differences outside this region of the distribution will be rejected in the analysis algorithm. Estimation of the center of this peak gives the spacecraft range and range error.

The components of the range error are listed in Table 3. Most of the error terms are random and will be reduced by the square root of the number of independent measurements. A separate measurement can be made for each uplink pulse occurring at the rate of 63 Hz. The largest random errors are due to photon statistics, so each measurement should be independent for those errors. The random instrumental errors may decrease more slowly since there may be correlation times longer than the interval between pulses. A bias error is introduced by the uncertainty in the troposphere delay derived from a model of the

troposphere and meteorological measurements. Other systematic errors include the ground station and transceiver instrumental biases. Instrumental errors are often given in time units. Since each time error contributes to the round-trip light time error, the range error is given by 1/2 the time error times the speed of light.

The start time error is associated with the time tagging of a sample of the uplink pulse. Relying on the experience of SLR measurements, it is supposed that the ground station systematic errors can be calibrated, by using a fixed reference or a well-known Earth-orbiting target, to a level below the troposphere bias error. The random detection errors come from the photon statistics, the PMT jitter, and the electronics jitter. The photon statistical error for the downlink reception derived in Section IV was 0.38 nsec, corresponding to 5.7 cm. For simplicity, the same value is used for the statistical component of the start time, although a stronger signal could be available. The PMT jitter for a 27 photoelectron event of 3.3 cm is taken from SLR measurements [10]. SLR systems may use a constant-fraction discriminator (CFD) following the PMT, with 0.2 cm error [10]. Here a value of 100 ps or 1.5 cm is included, representing 1/10 of the rise time of a shaping amplifier with 1 GHz bandwidth. The Hewlett Packard 5370A time interval unit has 100 ps accuracy [10], which is included here as the time-tag error.

The troposphere bias error is 1 cm at zenith for the SLR troposphere model [18]. The error will be different on the uplink and the downlink since several hours may separate them. Two-color measurements, possibly to an Earth-orbiting satellite, could be used to reduce the troposphere bias error if required. The fluctuating component of the troposphere is not very important for the two-way range measurements [19].

The photon statistical error at the spacecraft was discussed in Section IV. The 1.3-nsec error corresponds to a range error of 19 cm. The dark-count rate of the detector is ignored here since for some APDs the dark count can be made as low as 100/sec [15], which is lower than the uplink background rate. For the APD jitter, a value of 2.3 cm is used, which is the upper limit reported by Cova [14]. The output from an over-biased APD is assumed to be input to a CFD with a jitter of 0.2 cm. For ranging purposes, the discriminator output could be input directly to the laser modulator driver. The path time from the APD to the modulator driver can be quite short, perhaps 10–20 nsec. With proper temperature control and testing, the systematic delay error may be about 1 percent of the delay, corresponding to 3 cm. This value is entered as the electronics bias in Table 3. The error between triggering the laser modulator and the output light pulse depends on the laser design. Table 3 includes 23 cm (1.5 nsec) for the random error that is reported for a particular cavity-switched laser used for SLR [10]. The systematic error in the modulator driver can be calibrated out in SLR systems. For the spacecraft laser, an appropriate error will have to be derived from tests on candidate lasers. A value of 0.2 nsec (10 percent of the rise time) is included in Table 3 for the systematic laser error.

The downlink troposphere error is the same as the uplink error used above. The reception error is identical to the start-time error. The final error term in Table 3 is the clock error in keeping track of time between range transmission and reception. If the clock accuracy is 1 part in $10^{14}$ for the round-trip light time to Saturn, the range error is $10^{-14}$ times the Earth–Saturn distance (10 AU), which is 1.5 cm. Current hydrogen maser stabilities are better than this over the round-trip light time.[3]

Examination of the terms in Table 3 shows that the random errors drop below the few-centimeter level after a few seconds, assuming 63 independent measurements per second. Due to correlations between measurements, the instrumental errors may drop more slowly, but SLR results suggest that the random instrumental errors drop below the few-centimeter level in a reasonable time period (a few minutes). The systematic errors listed are at the few-centimeter level, indicating that an overall range error of less than 10 cm may be possible. This is comparable to the radio metric accuracy range one might achieve with a dual-frequency digitized system [20]. The most important unknown systematic effects are the detection algorithm and the laser modulator response. Tests of candidate spacecraft detectors and lasers will have to be performed to substantiate these numbers.

## VI. Range-Rate Error Budget

The two-way range algorithm used above returns 63 range points/sec. During 1 sec, the spacecraft moves on the order of 1 km, so a model for the spacecraft motion is needed to fit expected versus predicted range points. The difference in the range points can be fit to the model to produce a measurement of range rate. At present, radio metric Doppler data are the simplest and most reliable data type used in spacecraft navigation. However, the orbit analysis utilizes a Doppler measurement by inte-

[3] B. Gutierrez-Lucas, *Deep Space Network/Flight Project Interface Design Handbook, Volume I: Existing Capabilities,* JPL Publication 810-5, Rev. D, Section FTS-10 (internal document), Jet Propulsion Laboratory, Pasadena, California, 1988.

grating the measured velocity over a time interval to produce a difference in range at the times of the interval end points.[4] If the optical telemetry system provides accurate range reliably, there may be no need to derive a range-rate measurement.

A least-squares fit to a sequence of (independent) range points equally spaced in time (at 63 Hz) can be used to find the error in range rate. The error components of each range point are given in Table 3. However, most of the range bias terms do not contribute to the range-rate error. The troposphere bias enters only due to a change in elevation of the spacecraft; the resulting error is small compared to the fluctuating troposphere. The systematic instrumental errors contribute depending on their time dependence. Here they are ignored, and only the random range errors are considered as contributing to the range-rate error. The range-rate error $\sigma_v$ is given by [16]

$$\sigma_v^2 = \frac{12\sigma_r^2}{\Delta t^2 N^3} \tag{7}$$

where $\sigma_r^2$ is the root-sum-square (RSS) of the random range point errors, $\Delta t$ is the time interval between range points, and $N \gg 1$ is the number of range points. The value of $\sigma_r$ from Table 3 is 35 cm. With a rate of 63 Hz, the range-rate error is

$$\sigma_v = 1.5 \text{ cm/sec} \left(\frac{T}{\text{sec}}\right)^{-1.5} \tag{8}$$

The error derived from Eq. (8) is less than 1 mm/sec after a 30-sec integration time.

## VII. DOR Error Budget

For a DOR measurement, two stations time tag the reception of downlink pulses. Differences in arrival times between the two stations are calculated on a pulse-by-pulse basis, and the distribution of these differences is analyzed to determine the geometric delay. The photon statistical error on this delay results purely from the downlink time-of-arrival error at both stations. Since synchronization with the uplink is not required, the measurement can be made directly on the telemetry signal.

The errors for the DOR measurement are listed in Table 4. Since the downlink pulse rate is 14,000/sec, the statistical terms are insignificant after a 1-sec integration time. The dominant errors are the clock offset error and the troposphere bias at each station. The global positioning system (GPS) is expected to be able to provide time calibration to 1 nsec between stations [21], which corresponds to the 30 cm in Table 4. The GPS is also expected to establish the geocentric station coordinates to a few centimeters [22]. One alternative to GPS clock synchronization is fiber-optic connections between stations. Extending the fibers to several-hundred-kilometer baselines with the necessary stability is not currently possible, but may be in the future. Another alternative means of clock synchronization is to use a combination of two-way and three-way range measurements, as discussed in the next section. This method may be able to establish intercomplex timing to the few-centimeter level.

Assuming that the clock synchronization problem can be solved, optical DOR measurements with few-centimeter accuracy should be possible. The angular accuracy will then be limited by the length of the available baseline. A 3-cm DOR measurement over a 300-km baseline corresponds to a 100-nrad angular measurement, which is not as accurate as present very-long baseline interferometry measurements. Better angular resolution requires either lower troposphere errors (assuming the clock error can be reduced to the troposphere level) or longer baselines. A 3000-km baseline could fit in the continental U.S. and potentially could provide measurements of about 10 nrad. Mutual station visibility would be a concern since optical measurements are more susceptible to poor weather conditions.

## VIII. Clock Synchronization Using Range Measurements

This section describes a method for clock synchronization that is much like a differenced two-way range measurement. In fact, a differenced two-way range measurement can be derived from the same information. This particular set of measurements avoids the problem of short station overlap interval that occurs for a more straightforward differenced two-way range measurement [23]. This synchronization method is not unique to optical systems and may have been considered for radio metric systems. There are advantages to using this technique for the optical system: using the same instrumentation avoids local time-transfer stability problems, and this method could allow continual pointing at the spacecraft. The method is only outlined below. An error analysis would have to take into account the uncertainties in the motions of the Earth and the spacecraft, which are neglected here.

[4] T. Moyer, *Mathematical Formulation of the Double-Precision Orbit Determination Program (DPODP)*, JPL Technical Report 32-1527 (internal document), Jet Propulsion Laboratory, Pasadena, California, May 1971.

The sequence of measurements is shown in Fig. 6. Station A keeps time $t$, and station B keeps time $t'$. The difference in the clocks $\Delta\tau = t - t'$ is to be determined. Initially, the spacecraft sends a pulse that is detected by ground stations A and B. Each ground station records the time of pulse arrival (Fig. 6a). Station A records the time as $t_1$, while station B records the time as $t'_1$. After reception of the spacecraft pulse, each station sends up a pulse to the spacecraft, recording the times as $t_2$ and $t'_2$ (Fig. 6b). The time between downlink pulse reception and uplink transmission is taken to be short enough that the troposphere path delays at each station ($p_A$ and $p_B$) are the same for the uplink and the downlink. The spacecraft returns each uplink pulse after an instrumental path delay $s$. The times of reception of these two returned pulses are recorded at station A as $t_{3A}$ and $t_{3B}$ (Fig. 6c). In the meantime, station B could have set.

For the present, the rotation of the Earth and the motion of the spacecraft are ignored. Then two time-tag differences, $D_1$ and $D_2$, are formed as

$$D_1 = t_{3A} - t_2 = 2r_A/c + p_A + p_3 + s \quad (9)$$

$$D_2 = t_{3B} - t'_2 = r_A/c + r_B/c + p_B + p_3 + s + \Delta\tau \quad (10)$$

where $r_A$ is the distance from station A to the spacecraft, $r_B$ is the distance from station B to the spacecraft, $c$ is the speed of light, and $p_3$ is the media delay occurring on the final downlink from the spacecraft to station A (assumed to be the same for both downlinks). Taking the difference between these two values gives

$$D_3 = D_1 - D_2 = r_A/c - r_B/c + p_A - p_B - \Delta\tau \quad (11)$$

The regular DOR measurement gives

$$D = t_1 - t'_1 = r_A/c - r_B/c + p_A - p_B + \Delta\tau \quad (12)$$

Summing $D$ and $D_3$ gives a result equivalent to a differenced two-way range measurement. Subtracting $D_3$ from $D$ gives twice the clock offset $\Delta\tau$. Note that the tropospheric and geometric delays cancel out in the determination of the clock offset.

For this discussion of clock synchronization, instrumental delays were ignored along with Earth and spacecraft motions. However, since the method involves the same instrumentation as range measurements, the clock synchronization should approach the level of the range error. In fact, the error may be less since some of the error terms cancel out in the differences. Further analysis will have to be performed to make a better assessment of the clock synchronization accuracy. In practice, a method that involves three one-way light times to Saturn may not be desirable. It may be preferable to use a nearer spacecraft for clock synchronization and to perform DOR based on this clock synchronization on the deep-space probe.

## IX. Discussion

This article has attempted to consider in some detail the potential accuracy of optical two-way range, range rate, and DOR. The ranging system assumed for this analysis relies almost entirely on telemetry system hardware and can be implemented with little impact on telemetry system design. This analysis shows that, given a reasonable telemetry system, the photon statistical errors on the resulting range and DOR observations fall below the few-centimeter level within a few seconds of observation time. Other sources of random error exist, but can be reduced to the centimeter level within a few minutes of observation.

For two-way range measurements, the most important error sources are the troposphere delay uncertainty and the error in the spacecraft delay calibration. Since the spacecraft transceiver is in an early stage of development, the bias errors cannot be properly characterized here. However, there is reason to believe that careful design and calibration of the transceiver will allow two-way range accuracy to be 10 cm or less. For DOR measurements, the major errors are due to the troposphere and the calibration of the offset between station clocks. A method of measuring this clock offset has been proposed. Further work is needed to determine if it is feasible. If this or some other method of clock synchronization allows station clocks to be calibrated to the 30-ps level, then angular accuracy using DOR will be limited by the few-centimeter troposphere error and the length of the available baseline.

## Acknowledgments

The authors would like to thank J. M. Davidson and C. C. Chen for many suggestions that contributed to this work.

## References

[1] J. Lesh, "Deep Space Optical Communications Development Program," *Proc. SPIE*, vol. 756, pp. 8–11, 1987.

[2] E. L. Kerr, "Strawman Optical Reception Development Antenna (SORDA)," *TDA Progress Report 42-87,* vol. July–September 1986, Jet Propulsion Laboratory, Pasadena, California, pp. 97–110, November 15, 1986.

[3] E. L. Kerr, "Fraunhofer Filters to Reduce Solar Background for Optical Communications," *TDA Progress Report 42-93,* vol. January–March 1988, Jet Propulsion Laboratory, Pasadena, California, pp. 48–55, May 15, 1988.

[4] K. Cowles, "A Visibility Characterization Program for Optical Communication Through the Atmosphere," *TDA Progress Report 42-97,* vol. January–March 1989, Jet Propulsion Laboratory, Pasadena, California, pp. 221–225, May 15, 1989.

[5] S. G. Lambert et al., *Design and Analysis Study of a Spacecraft Optical Transceiver Package,* McDonnell Douglas Report for JPL Contract No. 957061, St. Louis, Missouri, 1985.

[6] W. K. Marshall and B. D. Burk, "Received Optical Power Calculations for Optical Communications Link Performance Analysis," *TDA Progress Report 42-87,* vol. July–September 1986, Jet Propulsion Laboratory, Pasadena, California, pp. 32–40, November 15, 1986.

[7] *Parametric Analysis of Microwave and Laser Systems for Communication and Tracking,* Hughes Aircraft Co., Report No. P67–09, 1966. Referenced in W. K. Pratt, *Laser Communications Systems,* New York: John Wiley and Sons, 1969.

[8] R. C. Ramsey, "Spectral Irradiance from Stars and Planets, above the Atmosphere, from 0.1 to 100.0 Microns," *Applied Optics,* vol. 1, pp. 465–472, 1962.

[9] I. L. Goldberg, *Radiation from Planet Earth,* U.S. Army Signal and Research Development Lab. Report 2231, AD-266-790, September 1961.

[10] J. J. Degnan, "Satellite Laser Ranging: Current Status and Future Prospects," *IEEE Trans. Geoscience and Remote Sens.,* vol. GE-23, pp. 398–413, 1985.

[11] M. Sasaki, "Satellite Laser Ranging at the Simosato Hydrographics Observatory and Its Preliminary Results," *J. Geodetic Soc. of Japan,* vol. 30, pp. 29–40, 1984.

[12] S. N. Del'nova, V. I. Markov, N. K. Smirnov, and N. A. Krivokul'skaya, "Characteristics of Multialkali Photomultipliers with Total Internal Reflection," *Instruments and Experimental Techniques,* vol. 24, pp. 1269–1272, 1981.

[13] Data sheet for RCA C30954E photodiode, RCA Corporation, Ste. Anne de Bellevue, Quebec, Canada H9X–3L3, 1979.

[14] S. Cova, A. Longoni, and A. Andreoni, "Towards Picosecond Resolution with Single-Photon Avalanche Diodes," *Rev. Sci. Inst.*, vol. 52, pp. 408–412, 1981.

[15] R. G. W. Brown, K. D. Ridley, and J. G. Rarity, "Characterization of Silicon Avalanche Photodiodes for Photon Correlation Measurements. 1: Passive Quenching," *Applied Optics,* vol. 25, pp. 4122–4126, 1986.

[16] P. R. Bevington, *Data Reduction and Error Analysis for the Physical Sciences,* New York: McGraw-Hill, 1969.

[17] M. Fisz, *Probability Theory and Mathematical Statistics,* New York: John Wiley and Sons, 1963.

[18] J. B. Abshire and C. S. Gardner, "Atmospheric Refractivity Corrections in Satellite Laser Ranging," *IEEE Trans. Geoscience and Remote Sens.*, vol. GE–23, pp. 414–425, 1985.

[19] C. S. Gardner, "Effects of Random Path Fluctuations on the Accuracy of Laser Ranging Systems," *Applied Optics,* vol. 15, pp. 2539–2545, 1976.

[20] L. E. Young, "Improved Ranging Systems," Workshop on Relativity and Gravitational Experiments, Annapolis, Maryland, June 1988 (unpublished).

[21] G. Blewitt, "Carrier Phase Ambiguity Resolution for the Global Positioning System Applied to Geodetic Baselines up to 2000 km," *J. Geophysical Research,* vol. 94, pp. 10187–10203, 1989.

[22] R. P. Mala and S.-C. Wu, "Deriving a unique reference frame for GPS measurements," *IEEE Position Location and Navigation Symposium Record,* pp. 177–184, 1988.

[23] T. H. Taylor, J. K. Campbell, R. A. Jacobson, B. Moultrie, R. A. Nichols, and J. E. Riedel, "Performance of Differenced Range Data Types in Voyager Navigation," *Journal of Guidance, Control, and Dynamics,* vol. 7, pp. 301–306, May–June 1984.

**Table 1. Downlink telemetry system parameters**

| Parameter | Value |
|---|---|
| Wavelength, $\mu$m | 0.532 |
| Average laser output power, W | 2.000 |
| Diameter of XMTR aperture, m | 0.300 |
| Obscuration diameter of XMTR, m | 0.060 |
| Transmitter optics efficiency | 0.650 |
| XMTR pointing bias error, $\mu$rad | 0.300 |
| XMTR rms pointing jitter, $\mu$rad | 0.300 |
| Diameter of RCVR aperture, m | 10.000 |
| Obscuration diameter of RCVR, m | 4.300 |
| Receiver optics efficiency | 0.380 |
| Narrowband filter transmission factor | 0.400 |
| Filter spectral bandwidth, Å | 0.300 |
| Detector quantum efficiency | 0.350 |
| Detector field-of-view angle, $\mu$rad | 100.000 |
| Background, W/$\mu$m m$^2$ str | 100.000 |
| Number of slots per PPM symbol | 256.000 |
| Data rate, kbits/sec | 114.350 |
| Pulse rate, number of symbols/sec | 14294.000 |
| Slot width, nsec | 10.000 |
| Distance between XMTR and RCVR, AU | 10.000 |
| Atmospheric transmission factor | 0.500 |
| Detected signal photons/pulse | 27.600 |
| Detected background photons/slot | 2.150 |

**Table 2. Uplink telemetry system parameters**

| Parameter | Value |
|---|---|
| Wavelength, $\mu$m | 1.06 |
| Average laser output power, W | 110.00 |
| Diameter of XMTR aperture, m | 0.05 |
| Obscuration diameter of XMTR, m | 0.00 |
| Transmitter optics efficiency | 0.65 |
| XMTR pointing bias error, $\mu$rad | 2.50 |
| XMTR rms pointing jitter, $\mu$rad | 5.00 |
| Diameter of RCVR aperture, m | 0.30 |
| Obscuration diameter of RCVR, m | 0.06 |
| Receiver optics efficiency | 0.65 |
| Narrowband filter transmission factor | 0.80 |
| Filter spectral bandwidth, Å | 10.00 |
| Detector quantum efficiency | 0.10 |
| Detector field-of-view angle, $\mu$rad | 8.62 |
| Background, W/$\mu$m m$^2$ str | 6.50 |
| Number of slots/PPM symbol | 256.00 |
| Data rate, kbits/sec | 0.50 |
| Pulse rate, number of symbols/sec | 63.00 |
| Slot width, nsec | 10.00 |
| Distance between XMTR and RCVR, AU | 10.00 |
| Atmospheric transmission factor | 0.50 |
| Detected signal photons/pulse | 5.47 |
| Detected background photons/slot | $7.14 \times 10^{-5}$ |

**Table 3. Two-way range error budget[a]**

| Error source | Value |
|---|---|
| Start time error | |
| Instrumental biases | <3.0 cm |
| Detection statistics | 5.7 cm/$\sqrt{N}$ |
| PMT jitter | 3.3 cm/$\sqrt{N}$ |
| Amplifier jitter | 1.5 cm/$\sqrt{N}$ |
| Time-tag error | 1.5 cm/$\sqrt{N}$ |
| Uplink troposphere error | |
| Bias component | 1.0 cm/sin $E$ |
| Fluctuating component | 0.1 cm/$\sqrt{(N \sin E)}$ |
| Spacecraft turnaround error | |
| Detection statistics | 19.0 cm/$\sqrt{N}$ |
| APD jitter | 2.3 cm/$\sqrt{N}$ |
| Discriminator jitter | 1.5 cm/$\sqrt{N}$ |
| Electronics bias | 3.0 cm |
| Modulator random error | 23.0 cm/$\sqrt{N}$ |
| Modulator bias error | 7.5 cm |
| Downlink troposphere error | |
| Bias component | 1.0 cm/sin $E$ |
| Fluctuating component | 0.1 cm/$\sqrt{(N \sin E)}$ |
| Reception time error | |
| Instrumental biases | <3.0 cm |
| Detection statistics | 5.7 cm/$\sqrt{N}$ |
| Detector jitter | 3.3 cm/$\sqrt{N}$ |
| Amplifier jitter | 1.5 cm/$\sqrt{N}$ |
| Time-tag error | 1.5 cm/$\sqrt{N}$ |
| Clock rate error | <1.5 cm |

[a] $N$ is the number of independent measurements, which may be different for instrumental and troposphere errors (which may have correlated noise) and detection errors (which are purely statistical). The elevation angle is $E$.

**Table 4. DOR error budget[a]**

| Error source | Value |
|---|---|
| Station 1 detection error | |
| Instrumental bias | <3.0 cm |
| Detection statistics | 5.7 cm/$\sqrt{N}$ |
| Detector jitter | 3.3 cm/$\sqrt{N}$ |
| Amplifier jitter | 1.5 cm/$\sqrt{N}$ |
| Time-tag error | 1.5 cm/$\sqrt{N}$ |
| Troposphere bias | 1.0 cm/sin $E$ |
| Troposphere fluctuation | 0.1 cm/$\sqrt{(N \sin E)}$ |
| Station 2 detection error | |
| Instrumental bias | <3.0 cm |
| Detection statistics | 5.7 cm/$\sqrt{N}$ |
| Detector jitter | 3.3 cm/$\sqrt{N}$ |
| Amplifier jitter | 1.5 cm/$\sqrt{N}$ |
| Time-tag error | 1.5 cm/$\sqrt{N}$ |
| Troposphere bias | 1.0 cm/sin $E$ |
| Troposphere fluctuation | 0.1 cm/$\sqrt{(N \sin E)}$ |
| Clock offset error | 30.0 cm |

[a] $N$ is the number of independent measurements, and $E$ is the elevation angle.

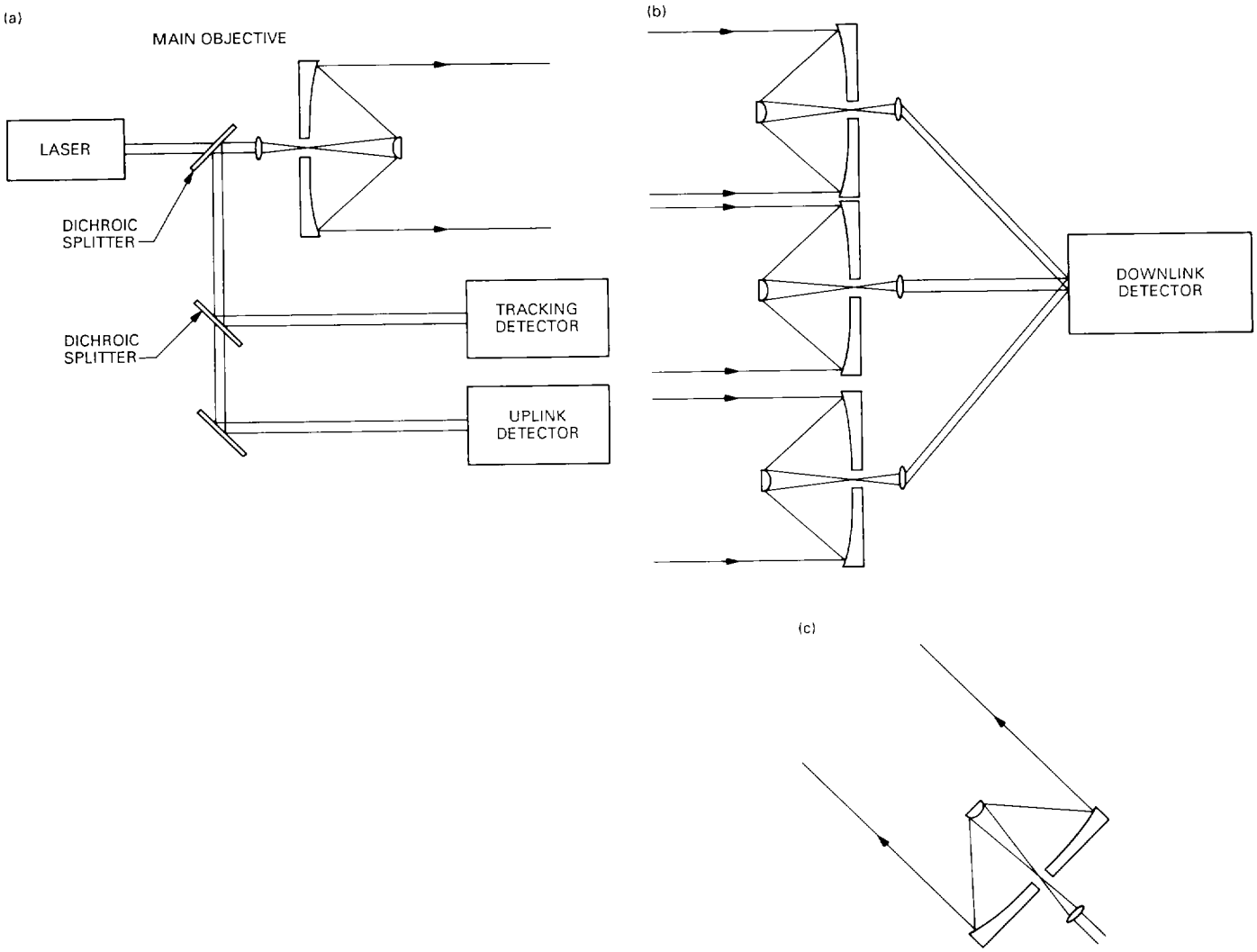


**Fig. 1. Simplified optical diagram for PPM telemetry system: (a) spacecraft transceiver; (b) ground receiver; and (c) uplink transmitter.**

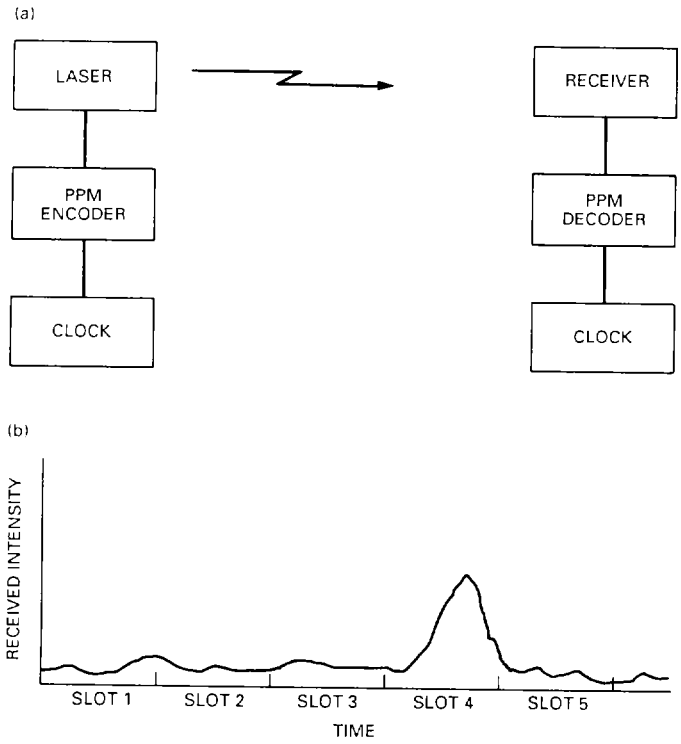


**Fig. 2. PPM modulation method schematic: (a) telemetry system; and (b) received intensity diagram.**

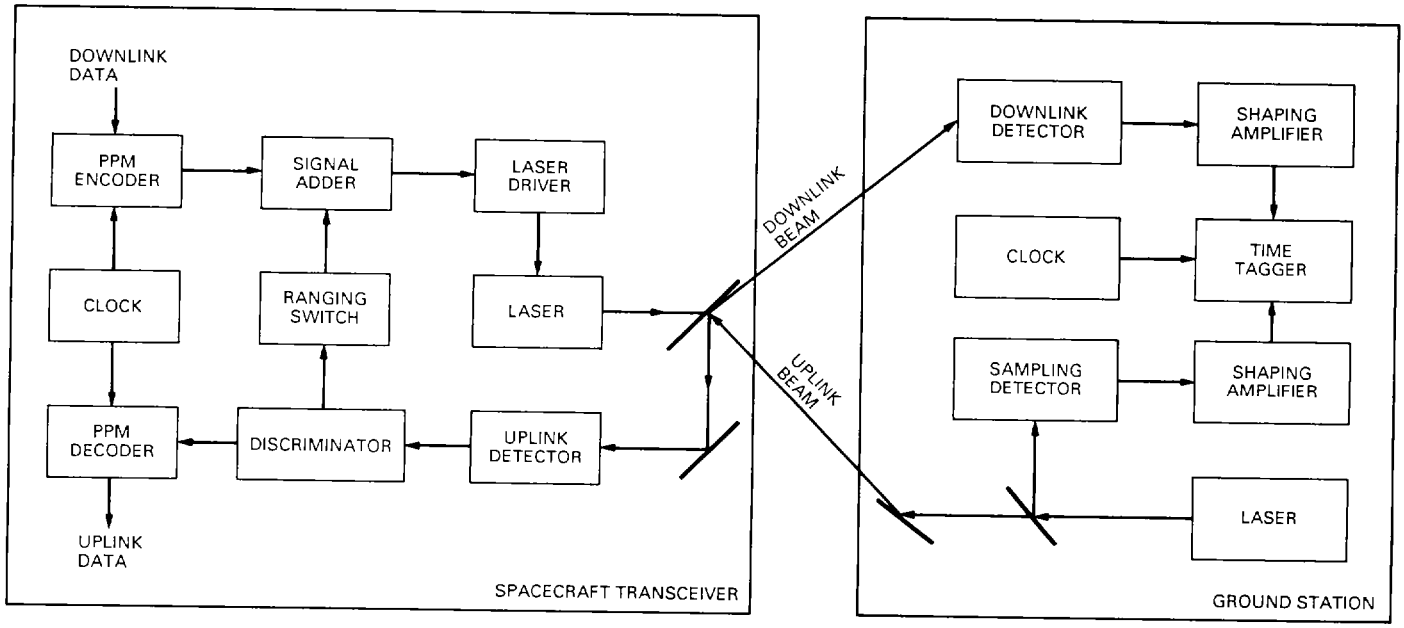


**Fig. 3. Two-way range measurement.**

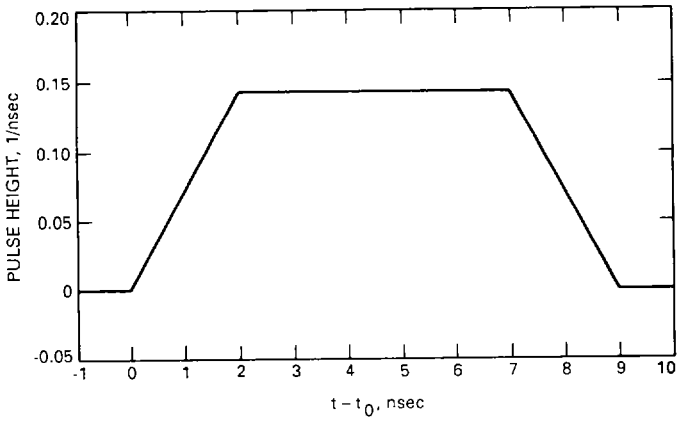


**Fig. 4. Normalized laser output pulse shape.**

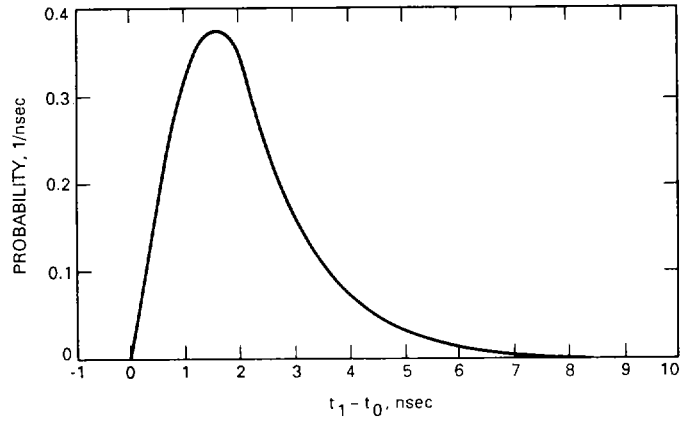


**Fig. 5. Normalized probability distribution for detection of first photon.**

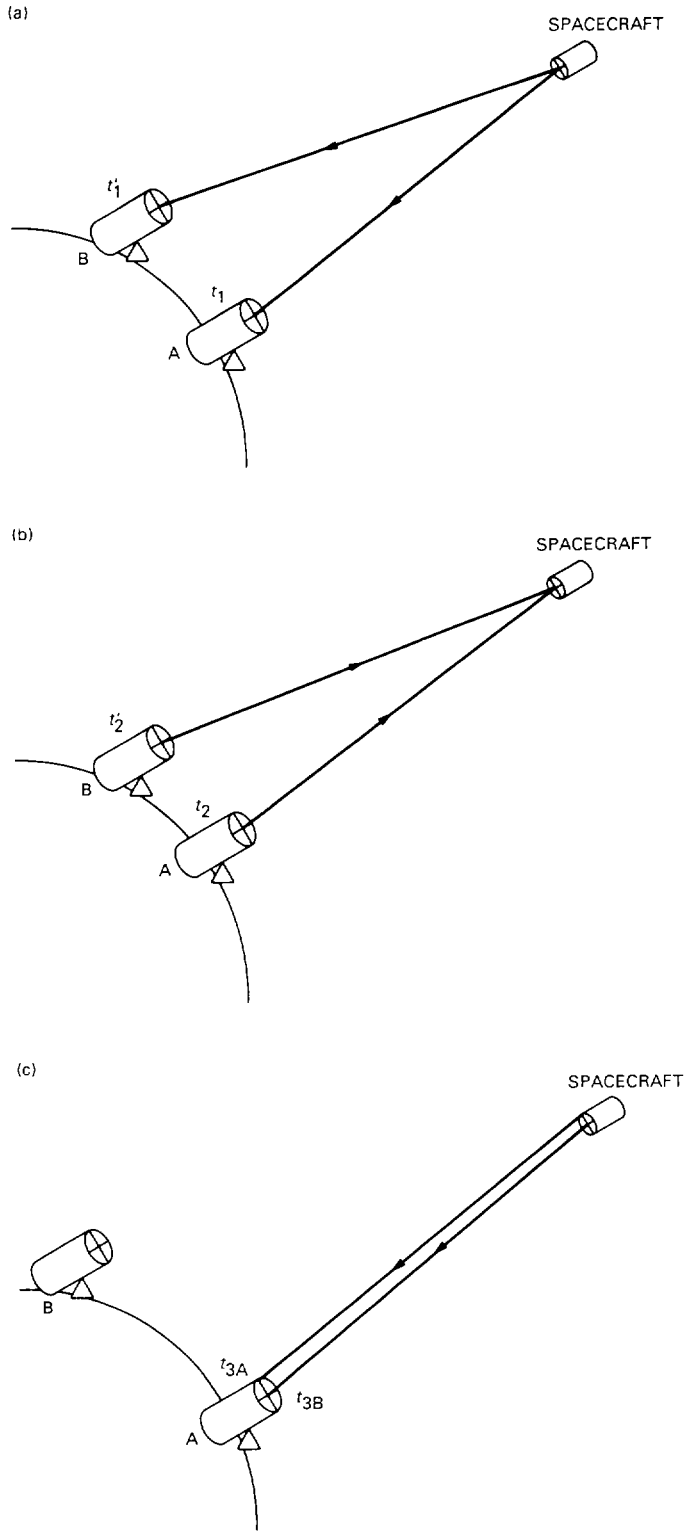


**Fig. 6. Sequence of events (time tags) for clock synchronization: (a) initial downlink; (b) both stations send uplink; and (c) station A records time of return for both uplinks.**